Computer Methods in Biomechanics and Biomedical Engineering,
Vol. 00, No. 00, January 2007, 1–15

The phenomenon of twisted growth: Humeral torsion in dominant arms of high performance tennis players

R.E. TAYLOR[†], C. ZHENG[†], R.P. JACKSON[♯], J.C. DOLL[†], J.C. CHEN[♯], K.R.S. HOLZBAUR[⋆], T. BESIER[‡], E. KUHL[*†♯]

[†] Department of Mechanical Engineering, Stanford University, Stanford, CA 94305, USA
[♯] Department of Bioengineering, Stanford University, Stanford, CA 94305, USA
[‡] Department of Orthopaedic Surgery, Stanford University, Stanford, CA 94305, USA
[⋆] Department of Biomedical Engineering, Wake Forest University School of Medicine, Winston-Salem, NC 27157, USA

(*v3.1 released May 2007*)

This manuscript is driven by the need to understand the fundamental mechanisms that cause twisted bone growth and shoulder pain in high-performance tennis players. Our ultimate goal is to predict bone mass density in the humerus through computational analysis. The underlying study spans a unique complete four level analysis consisting of a high speed video analysis, a musculoskeletal analysis, a finite element based density growth analysis and an X-ray based bone mass density analysis. For high performance tennis players, critical loads are postulated to occur during the serve. From high speed video analyses, the serve phases of maximum external shoulder rotation and ball impact are identified as most critical loading situations for the humerus. The corresponding posts from the video analysis are reproduced with a musculoskeletal analysis tool to determine muscle attachment points, muscle force vectors and overall forces of relevant muscle groups. Collective representative muscle forces of the deltoid, latissimus dorsi, pectoralis major and triceps are then applied as external loads in a fully three dimensional finite element analysis. A problem specific nonlinear finite element based density analysis tool is developed to predict functional adaptation over time. The density profiles in response to the identified critical muscle forces during serve are qualitatively compared to X-ray based bone mass density analyses.

Keywords: bone mass density changes, functional adaptation, musculoskeletal analysis, finite element analysis, sports medicine

1. Motivation

On September 27, 2004 Andy Roddick hit the current world record 155 mph serve in his Davis Cup match against Belarus which set him up with three match points against Vladimir Voltchkov. By that time, at 22 years of age, Roddick had broken his own speed record for the third time. In tennis, like in almost all other high performance sports, there is a tendency that professional athletes tend to reach their peak performance at a much younger age than they used to several decades ago. Accordingly, athletes have to start full-time practice in their early childhood which strongly overlaps with the period of skeletal and muscular development. It is the responsibility of their coaches and physicians to design efficient training programs targeted at maximal performance and minimal risk of injury. Biomechanics can play a crucial role in supporting the design of these training strategies. Understanding the body's response to critical mechanical loads during serve or groundstroke is essential for success. By predicting the functional adaptation of bones and muscles,

*Corresponding author. Email: ekuhl@stanford.edu

Computer Methods in Biomechanics and Biomedical Engineering
ISSN: 1741-5977 print/ISSN 1741-5985 online
http://www.tandf.co.uk/journals
DOI: 10.1080/1741597YYxxxxxxxx

biomechanics simulation can help to explain and eventually prevent common forms of injuries caused by chronic overuse.

From a scientific point of view, tennis players as well as baseball pitchers and handball players are extremely popular study subjects for functional adaptation and bone hypertrophy since their two arms provide both an active hypertrophic response and a passive control all within the same individual. Severe functional adaptation in the form of increased humeral retrotorsion and twisted bone growth due to extensive external and internal rotation of the dominant arm of elite tennis players has been reported by Chandler et al. (1990); Krahl et al. (1994); Haapasalo et al. (2000); Ducher et al. (2005); Elliott (2006). The same phenomenon can be found in baseball pitchers, see Sabick et al. (2004); Osbahr et al. (2002), or handball players, see Pieper (1998). Proximal growth and remodeling of the humerus and adaptation-induced inter-arm asymmetry are more pronounced, but unfortunately also significantly more injurious, when athletes begin their intensive training during early stages of skeletal and muscular development, see Chandler et al. (1990); Krahl et al. (1994); Ducher et al. (2005).

Figure 1. Kinetic chain during serve recorded by high speed video analysis. Typical sequence covers four characteristic phases: (I) backswing, (II) maximum external shoulder rotation, (III) ball impact and (IV) maximum internal shoulder rotation. Muscle forces on the humerus are postulated to be highest during maximum external shoulder rotation and ball impact.

How can an athlete possibly accelerate an object to 155 mph? To be able to improve performance, identify the critical loads and interpret the potential risk factors during a tennis serve, it is important to fully understand the kinetic chain, i.e., the efficient function and interaction of all body parts involved in stroke production, see Elliott (2006); Elliott et al. (2003). Figure 1 displays a typical kinetic chain during serve. According to the studies of Elliott et al. (1995), the individual contributions to maximum racket velocity at impact are a sum of 10% shoulder activity, 15% upper arm horizontal flexation, 40% upper arm internal rotation, 5% forearm prognation and 30% hand flexation. This underlines the significant role of the internal rotation of the upper arm at the shoulder joint during service. Enormous muscle forces are involved in these activities and it is not surprising that most high performance tennis players suffer from acute or chronic shoulder pain, see, e.g., Elliott et al. (2003); Hill (1983); McCann and Bigliani (1994).

How are these tremendous muscle forces generated? The optimal activation of muscle force can be achieved in a balanced interplay of stretch and shortening as described in detail in Noffal (1999). During the eccentric pre-stretch phase, elastic energy is stored in the anterior shoulder muscles. When timed correctly, this energy can be partially recovered during the concentric phase of muscle shortening such that the overall muscle performance is enhanced. The internal rotators, in particular the pectoralis major and the latissimus dorsi, must accelerate the upper arm in the swing to impact and thereby apply a giant internal rotational torque at the proximal end of the humerus. At the distal end of the humerus, the forearm is creating an external rotation torque. The net result is a torque about the long axis of the humerus. It was previously postulated that during ball contact, mechanical stimuli in form of vibrations are transmitted from the racket to the hand and initiate functional adaptation, see Krahl et al. (1994). In this manuscript, however,

we illustrate that it is the above described stretch-shortening interplay of the internal rotators that generates the most critical loading scenario for bone growth and remodeling. In response to this overload, humerus density increases locally to maintain bone-muscle-force equilibrium and avoid tissue overuse that might otherwise result in acute or chronic shoulder pain.

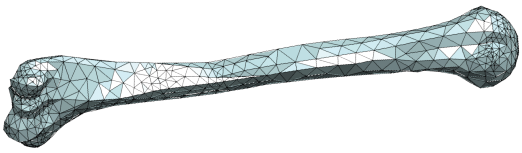

Figure 2. Right humerus. The proximal humerus (right) consists of a large rounded head of nearly hemispherical form. The humerus shaft is almost cylindrical in its superior half (right) and prismatic and fattened below (left). The inferior extremity of the humerus (left) is flattened and slightly curved forward ending below in a broad articular surface which is divided by a slight ridge.

How can the effects of torsional humeral loading be quantified? One of the first rigorous studies of torsion in the human humerus was conducted by Krahl (1947). Based on systematic analyses with the help of a torsiometer, Krahl concluded that twisted humeral geometry at different stages of development could be attributed to muscle forces inducing a torsional load. Inter-arm asymmetry in high performance athletes was addressed by Jones et al. (1977) in a qualitative investigation of humeral hypertrophy based on X-ray images of tennis player arms. Amongst their 84 study subjects, the cortical thickness of the dominant arm in male tennis players was 34.9% larger as compared to the control side, in women they found a difference of 28.4%. Surprisingly, even though the experimental techniques have become more advanced nowadays, the general tendency of one-sided bone hypertrophy remains the same, see, e.g., Ducher et al. (2005). Through radiologic investigations of athletes who started training in their early childhood, Krahl et al. (1994) not only found an increase in bone density and bone diameter in response to active training but also a pronounced increase in length of the dominant arm. Based on radiographic studies, Osbahr et al. (2002) classified this functional adaptation in bone to be predominantly of rotational nature.

How can the stress and the functional adaptation of the humerus be predicted? Approximately three decades ago, Cowin and Hegedus (1976) developed the first theory of adaptive elasticity to characterize mechanically driven growth in hard tissues. The influence of torsional loading was first elaborated analytically by Cowin (1987) based on an idealized cylindrical model of the diaphyseal region of long bone. Since then, Cowin's theory has been modified and refined by many researchers see, e.g., Beaupré et al. (1990); Harrigan and Hamilton (1992); Jacobs et al. (1995); Carter and Beaupré (2001); Kuhl and Steinmann (2003a,b); Kuhl and Balle (2005); Kuhl et al. (2003). Nevertheless, the fundamental ideas remain the same in all theories: a mechanical driving force, energy, stress or strain, initiates a local increase or decrease of density until a biological equilibrium state is reached. Changes in loading stimulate functional adaptation and the density profile is adjusted accordingly. While Cowin's original analyses are merely analytical, more recent work is based on computational simulations allowing for a more sophisticated nonlinear characterization of growth and a more accurate representation of bone geometry. The ultimate goal is to predict fully three dimensional patient specific density profiles that could be compared to bone mass density index measurements. Theoretically, the underlying finite element simulation tool not only allows for a precise modeling of bone geometry but could also account for an accurate representation of the individual muscle forces acting on the bone. It is difficult, however, to correctly measure these forces in vivo. Musculoskeletal simulation provides a powerful tool

to determine muscle force vectors in silico, see Delp et al. (2007a,b). These force vectors are essential input parameters for the finite element based bone density simulation, see Kuhl (2007).

Motivated by athlete college tennis players who reported chronic pain in their dominant shoulder, we aim at predicting humeral growth in the stroke arm in response to high performance sport specific mechanical loads. To this end, we develop a finite element based computational tool to simulate the functional adaptation in hard tissues in response to mechanical load or, in particular, sport specific overload. We postulate that the critical load scenario that initiates bone growth and remodeling is related to maximum external shoulder rotation associated with maximum pre-stretch of the internal rotators. To test this assumption, we compare the computationally predicted density profiles in response to the two loading scenarios of maximum external shoulder rotation and ball impact. Section 2 describes how the relevant muscle forces during both scenarios are determined by reproducing critical postures from video analysis. These muscle forces are then applied as external loads in fully three dimensional, nonlinear finite element bone density analysis to predict density changes in response to loading. Section 3 summarizes the results of the finite element simulation for the critical load cases during service. The potential impact of this research is discussed in section 4.

2. Methods

In this section, we describe the sequence of tools we applied to generate the input for the finite element simulation of humeral growth. To test the assumption that peak loading conditions relevant to growth occur at maximum external shoulder rotation rather than at ball impact, we first elaborate the high speed video analysis during serve. Based on the individual images, we identify significant postures to determine critical humerus muscle forces. In particular, we focus on two stages during the serve: maximum external shoulder rotation and ball impact. Their postures are reproduced with the open source software OpenSim that provides muscle attachment points and allows to determine relevant muscle forces. These generated loads are then applied as external forces in a finite element analysis to predict changes in bone density in response to overload. The calculated density profiles are qualitatively compared to bone mass density measures of the study subject.

2.1. *High speed video analysis*

High speed video analysis was carried out in the Human Performance Lab at Stanford University. Figure 3 shows a sequence of snapshots during service as recorded with two synchronized cameras. The upper and lower row display the frontal and the lateral view, respectively. The sequence covers the phases of (I) backswing, (II) maximum external shoulder rotation, (III) ball impact and (IV) maximum internal shoulder rotation, figure 3, from left to right.

During the serve, the entire upper limb is subject to tremendous loads. Figures 3.I and 3.II illustrate the backswing phase. At the late stage of backswing, the upper arm takes an extreme external position. In fact, this posture is associated with such extreme limits of shoulder joint range motion that it can only be reached dynamically. This cocked position serves to pre-stretch the internal rotators prior to stroke. Figures 3.II and 3.III display how maximum forces are generated at ball impact: Maximum acceleration is created by the superposition of a shoulder-over-shoulder trunk rotation about the red axis and an explosive internal rotation of

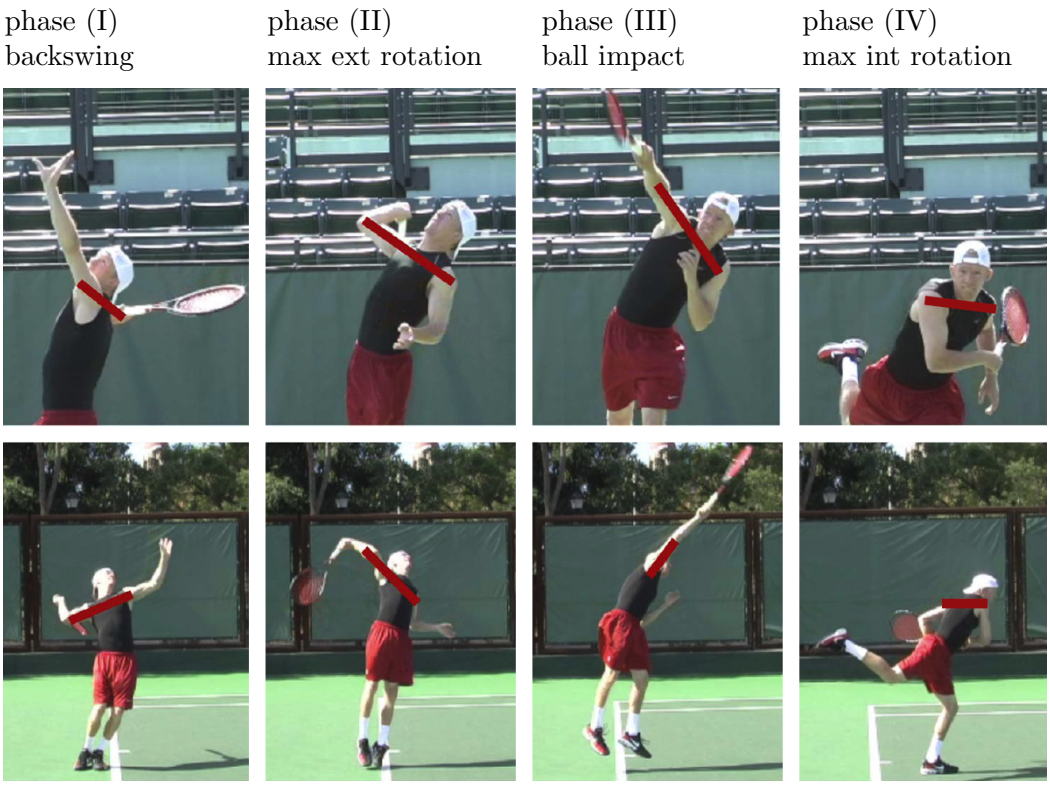

Figure 3. Four phases during high speed serve: (I) backswing, (II) maximum external shoulder rotation (III) ball impact and (IV) maximum internal shoulder rotation (from left to right). The upper series displays the frontal view, the lower series the corresponding lateral view. Critical muscle forces are hypothesized to occur at phase (II) maximum external shoulder rotation and at phase (III) ball impact. As illustrated through the red axes, the humerus remains aligned with the shoulders throughout the entire serve indicating that forces are generated primarily through a rotational motion.

the humerus at the shoulder joint generated by the concentric contraction of the internal rotators. After ball impact, between figures 3.III and 3.IV, the contraction of the internal rotators is slowed by contraction of the external rotators during the follow-through phase. We postulate that critical forces occur during phase (II) at maximum external shoulder rotation and phase (III) at ball impact.

2.2. *Musculoskeletal analysis*

In the second step of our analysis, we duplicate the critical postures of figures 3.II and 3.III within the open source software OpenSim, see Delp et al. (2007a). We apply OpenSim's upper limb model which represents a 50th percentile male with average muscle properties. Its humerus, radius and ulna were manually digitized from cadaveric specimen as described in Holzbaur et al. (2005, 2007). The model allows the determination of forces in response to the generated postures and moments arms. It is essentially based on a four parameter Hill-type muscle model in terms of the optimal fiber length, the peak force, the tendon slack length and the pennation angle, see Holzbaur et al. (2005) for details.

We identify four critical load groups on the humerus: deltoid, latissimus dorsi, pectoralis major and triceps. While the former three muscle groups connect the humerus to the torso, the latter group extends to the forearm. Due to its particular location on the lateral side, this muscle group is significantly stretched during maximum external shoulder rotation as illustrated in figure 4 (top, right). The same is true for the internal rotators, in particular the pectoralis major, which is stretched remarkably at the late stages of backswing.

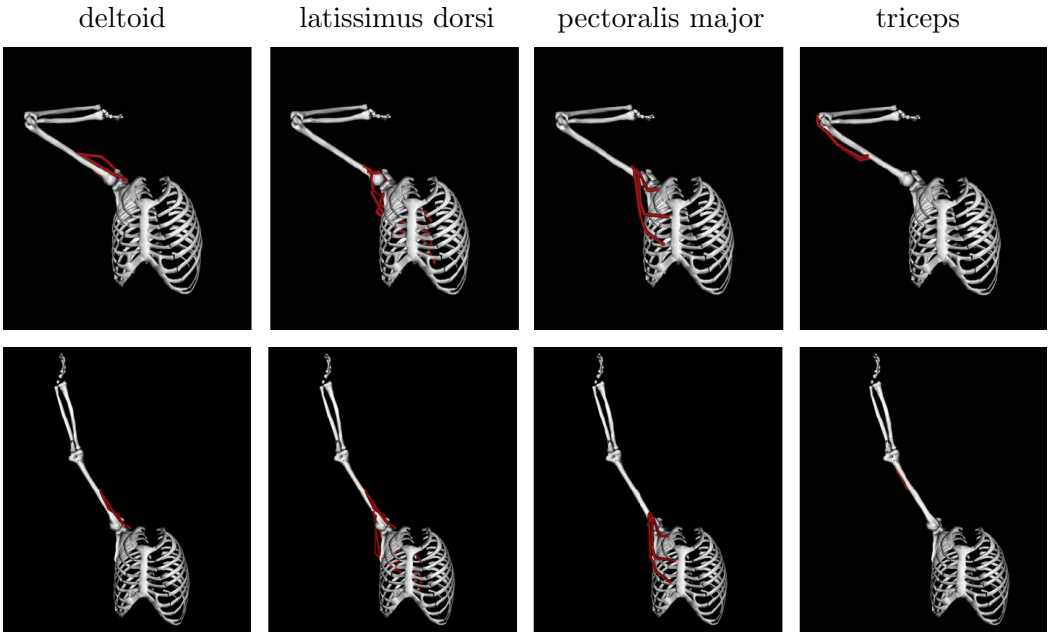

Figure 4. Relevant muscle groups of right humerus: deltoid, latissmus dorsi, pectoralis major and triceps (from left to right). All forces acting on the humerus during phase (II) maximum external shoulder rotation (top row) and phase (III) ball impact (bottom row) are summarized collectively in four representative force vectors.

Table 1. Representative muscle force vectors of right humerus: deltoid, latissmus dorsi, pectoralis major and triceps. All forces acting on the humerus during phase (II) maximum external shoulder rotation and phase (III) ball impact are summarized collectively in four representative force vectors.

load case	deltoid	latissimus dorsi	pectoralis major	triceps
phase (II)	1410 N	1275 N	1490 N	1250 N
	[+0.46, +0.76, −0.46]	[+0.49, +0.39, −0.78]	[+0.47, +0.75, −0.47]	[−0.44, −0.79, +0.44]
phase (III)	1600 N	1385 N	1170 N	580 N
	[+0.26, +0.94, −0.22]	[−0.57, +0.79, −0.23]	[+0.41, +0.82, −0.41]	[−0.25, −0.94, +0.25]

Similar to the classical bone adaptation analysis in the proxima femur, see e.g. Carter and Beaupré (2001); Kuhl et al. (2003), the relevant muscle forces are summarized collectively in four force vectors acting on the humerus during maximum external shoulder rotation and ball impact, see table 1. Actually, the musculoskeletal analysis provides detailed information about individual muscles of each muscle group as illustrated in figure 4. For the sake of transparency, however, these individual muscle forces are summarized collectively in four force vectors acting on the humerus during maximum external shoulder rotation and ball impact, see table 1. These force vectors are applied as external loads in the finite element analysis to determine overload induced humeral hypertrophy.

2.3. *Finite element growth analysis*

Bone density profiles in the right humerus in response to the critical muscle forces are determined with the help of a fully nonlinear finite element analysis tool. Figure 5 displays the finite element model of the right humerus subjected to the critical muscle forces resulting from the musculoskeletal analysis. Changes in the density ρ_0 are assumed to be driven by the neo Hookean free energy ψ_0^{neo} through the following biological equilibrium equation,

$$\mathrm{d}_t \rho_0 = \mathcal{R}_0 \quad \text{with} \quad \mathcal{R}_0 = c\,[\,[\rho_0/\rho_0^*]^{[n-m]}\psi_0^{\text{neo}} - \psi_0^*\,] \tag{1}$$

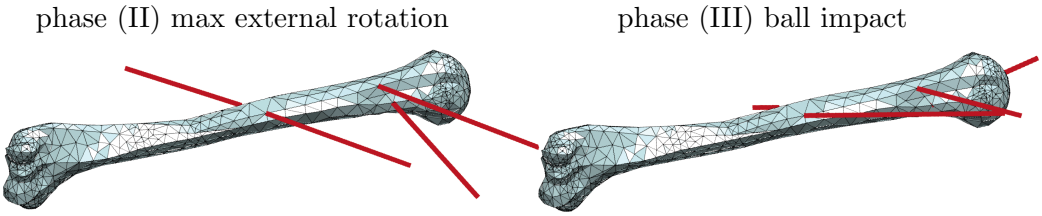

Figure 5. Finite element model of right humerus. Discretization with 1342 linear tetrahedral elements and 3969 degrees of freedom. Critical muscle forces of deltoid, latissimus dorsi, pectoralis major and triceps during phase (II) maximum external shoulder rotation (left) and phase (III) ball impact (right).

which, in fact, represents the balance of mass in open system thermodynamics. Its right hand side $\mathcal{R}_0$ constitutes a mass source that accounts for density changes. Based on the elastic free energy ψ_0^{neo}, the biological equilibrium equation basically predicts a local increase $\mathcal{R}_0 > 0$ or decrease $\mathcal{R}_0 < 0$ in density for overloaded or underloaded tissue regions, respectively. The constant c characterizes the speed of tissue adaptation, n and m are characteristic exponents that account for the porous nature of bone, ρ_0^* is the reference density and ψ_0^* the reference free energy or rather the biological stimulus. This energy driven format of growth dates back to the work of Harrigan and Hamilton (1992, 1993) and was found to render a stable growth predictions provided that $m > n$, see also Kuhl et al. (2003). Following Carter and Hayes (1977), we introduce the total free energy density ψ of the porous bone as the elastic free energy ψ^{neo} weighted by the relative density $[\,\rho_0 \,/\, \rho_0^*\,]^n$,

$$\psi = [\,\rho_0 \,/\, \rho_0^*\,]^n \,\psi^{\text{neo}} \quad \text{with} \quad \psi^{\text{neo}} = \tfrac{1}{2}\,\lambda\,\ln^2 J + \tfrac{1}{2}\,\mu\,[\,I_1 - n^{\text{dim}} - 2\,\ln J\,] \qquad (2)$$

which is a common approach for cellular materials, see also Gibson and Ashby (1997). Since we allow for finite kinematics, we use the neo Hookean free energy ψ^{neo} parameterized in terms of the deformation gradient $\boldsymbol{F} = \nabla\boldsymbol{\varphi}$ or, to be more precise, in terms of its first invariant $I_1 = \text{tr}\,(\boldsymbol{F})$ and its Jacobian $J = \det(\boldsymbol{F})$. Moreover, λ and μ are the two Lamé parameters and n^{dim} denotes the number of spatial dimensions. The free energy of equation (2) defines the Piola stress $\boldsymbol{P} = \partial_{\boldsymbol{F}}\psi$ that enters the mechanical equilibrium equation $\text{Div}(\boldsymbol{P}) \doteq \boldsymbol{0}$.

$$\boldsymbol{P} = [\,\rho_0 \,/\, \rho_0^*\,]^n \,\boldsymbol{P}^{\text{neo}} \quad \text{with} \quad \boldsymbol{P}^{\text{neo}} = \mu\,\boldsymbol{F} + [\,\lambda\,\ln J - \mu\,]\,\boldsymbol{F}^{-1}. \qquad (3)$$

With the above equations at hand, how do we determine the current density profile for the prescribed muscle forces? The evolution of the density $\rho_0^{\text{n+1}}$ at time $t^{\text{n+1}}$ is governed by the balance of mass of equation (1), a first order rate equation which has to be discretized in time. We suggest an unconditionally stable implicit Euler backward scheme based on the finite difference interpolation $\text{d}_t\rho_0 = [\,\rho_0^{\text{n+1}} - \rho_0^{\text{n}}\,] \,/\, \Delta t$. The discrete counterpart of equation (1) can then be cast into the following residual statement $\mathsf{R} = \rho_0^{\text{n+1}} - \rho_0^{\text{n}} - c\,[\,[\,\rho_0{}^{\text{n+1}} \,/\, \rho_0^*\,]^{[n-m]}\psi_0^{\text{neo}} - \psi_0^*\,]\Delta t \doteq 0$ which is obviously a nonlinear equation in terms of the current density $\rho_0^{\text{n+1}}$. We thus suggest an iterative solution strategy based on a local Newton iteration such that $\mathsf{R}_{\text{k+1}} = \mathsf{R}_{\text{k}} + \mathsf{dR}_{\text{k}}\,\Delta\rho_0 \doteq 0$. The linearization of the residual $\mathsf{dR}_{\text{k}} = \partial_{\rho_0}\mathsf{R}_{\text{k}} = c\,[n - m][\,\rho_0{}^{\text{n+1}} \,/\, \rho_0^*\,]^{[n-m]}\psi^{\text{neo}}\,\Delta t - 1$ renders the incremental update of the density as $\Delta\rho_0 = -\mathsf{R}_{\text{k}} \,/\, \mathsf{dR}_{\text{k}}$. The material density can then be updated as $\rho_0^{\text{n+1}} \leftarrow \rho_0^{\text{n+1}} + \Delta\rho_0$. The consistent linearization of Piola stress $\mathbf{A} = \text{d}_{\boldsymbol{F}}\boldsymbol{P}$ then renders the algorithmic

tangent operator

$$\begin{aligned} \mathbf{A} &= [\,\rho_0\,/\,\rho_0^*\,]^n\,\mathbf{A}^{\rm neo} + \gamma\,\boldsymbol{P}\otimes\boldsymbol{P} \\ \text{with}\quad \mathbf{A}^{\rm neo} &= \lambda \boldsymbol{F}^{-\rm t}\otimes\boldsymbol{F}^{-\rm t} + [\mu-\lambda\ln J]\boldsymbol{F}^{-\rm t}\underline{\otimes}\boldsymbol{F}^{-1} + \mu\boldsymbol{I}\,\overline{\otimes}\,\boldsymbol{I} \\ \text{and}\quad \gamma &= [\,c\,n\,[\,\rho_0/\rho_0^*\,]^{-m}]\,/\,[\,\rho_0 - c\,[n-m][\,\rho_0\,/\,\rho_0^*\,]^{[n-m]}\psi_0^{\rm neo}\,\Delta t\,] \end{aligned} \tag{4}$$

which ensures quadratic convergence of the global Newton iteration. Here, we have

Table 2. Computational algorithm to determine current density ρ_0 with the help of local Newton Raphson iteration scheme. Within a nonlinear finite element analysis, this iteration is embedded locally at the integration point level. At local convergence, the growth stresses $\boldsymbol{P}$ and growth tangent $\mathbf{A}$ are calculated to determine the element vector of internal forces and the element stiffness matrix for the global Newton Raphson iteration. At global convergence, equilibrium densities ρ_0 are stored locally as history variables on the integration point level.

compute elastic free energy	$\psi^{\rm neo}$	=	$1/2\lambda\ln^2 J + 1/2\mu\,[I_1 - n^{\rm dim} - 2\ln J]$
compute elastic stress	$\boldsymbol{P}^{\rm neo}$	=	$\mu\boldsymbol{F} + [\lambda\ln J - \mu]\boldsymbol{F}^{-1}$
compute elastic tangent	$\mathbf{A}^{\rm neo}$	=	$\lambda\boldsymbol{F}^{-\rm t}\otimes\boldsymbol{F}^{-\rm t} + [\mu-\lambda\ln J]\boldsymbol{F}^{-\rm t}\underline{\otimes}\boldsymbol{F}^{-1} + \mu\boldsymbol{I}\overline{\otimes}\boldsymbol{I}$
local Newton iteration			
compute residual	R	=	$\rho_0 - \rho_0^{\rm n} - c\,[\,[\rho_0/\rho_0^*]^{[n-m]}\psi^{\rm neo} - \psi_0^*\,]\,\Delta t$
compute derivative	dR	=	$1 - c\,[n-m][\rho_0/\rho_0^*]^{[n-m]}\psi^{\rm neo}/\rho_0\,\Delta t$
compute update	ρ_0	$\leftarrow$	$\rho_0 + \Delta\rho_0$ with $\Delta\rho_0 = -\mathsf{R}/\mathsf{dR}$
check convergence	$\lvert\Delta\rho_0\rvert$	$\leq$	tol ?
compute growth stress	$\boldsymbol{P}$	=	$[\rho_0/\rho_0^*]^n\,\boldsymbol{P}^{\rm neo}$
compute growth tangent	$\mathbf{A}$	=	$[\rho_0/\rho_0^*]^n\mathbf{A}^{\rm neo} + cn[\rho_0/\rho_0^*]^{-m}\Delta t/[\rho_0\mathsf{dR}]\boldsymbol{P}\otimes\boldsymbol{P}$

made use of the abbreviations $\overline{\otimes}$ and $\underline{\otimes}$ for the non–standard dyadic products according to the following component-wise definitions $\{\bullet\overline{\otimes}\circ\}_{ijkl} = \{\bullet\}_{ik}\otimes\{\circ\}_{jl}$ and $\{\bullet\underline{\otimes}\circ\}_{ijkl} = \{\bullet\}_{il}\otimes\{\circ\}_{jk}$. Also, for convenience, we have dropped the current time index such that $\rho_0 = \rho_0^{\rm n+1}$. The algorithm for an iterative determination of the current density ρ_0 is summarized in table 2.

To determine the critical loading situation for the humerus, two independent finite element simulations were performed for load scenarios (II) maximum external shoulder rotation and (III) ball impact. Although, of course, in vivo, growth is stimulated by a superposition of all relevant load cases, we analyze these two load cases separately to understand how bone would respond to each of them individually. The applied muscle forces from the deltoid, latissimus dorsi, pectoralis major and triceps for both loading scenarios are summarized in table 1 and illustrated in figure 5. Dirichlet boundary conditions are chosen in accordance with four contact areas between the humerus and the ulna and the radius on the distal end. On the proximal side, the contact area between the humerus and the shoulder joint is identified and fixed in space. The humerus is discretized by 1342 linear tetrahedral finite elements with a total of 3969 degrees of freedom. In the simulation, the Lamé parameters are chosen to $\lambda = 288.46$ and $\mu = 192.31$ corresponding to a Young's modulus of $E = 500$ N/mm^2 and Poisson's ratio of $\nu = 0.3$ in the linear limit. The initial density was normalized to $\rho_0 = 1.0$ g/cm^3, the biological stimulus is $\psi_0 = 0.01$ N/mm^2 and the exponents of growth are chosen to $m = 3.0$ and $n = 2.0$, respectively, see, e.g., Carter and Beaupré (2001); Kuhl et al. (2003). Because of the highly nonlinear nature of the coupled growth-deformation equations, the crit-

ical forces are applied in 10 time steps Δt each scaled by a factor 0.00025. Once the total forces are applied, another 54 time steps are calculated until biological equilibrium is reached.

2.4. *Bone density X-ray analysis*

To validate the computational prediction of density changes, we compare the finite element simulation with bone mineral density measurements of the right humerus.

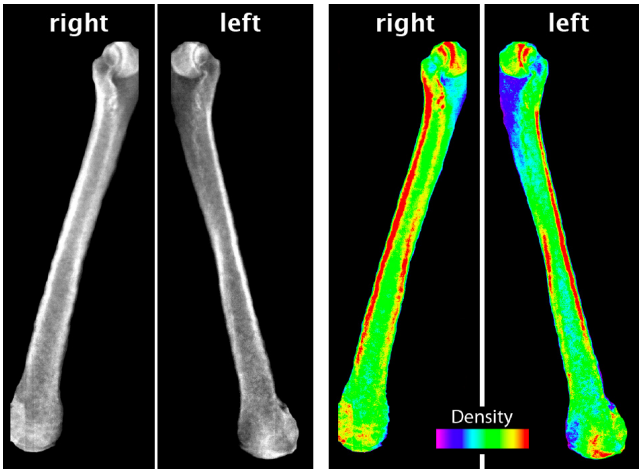

Figure 6. Representative X-ray images of right and left humerus of high performance tennis player. Dominant right arm clearly displays a higher bone mass density. Quantitative evaluation reveals a bone mass density index of 1.369 g/cm^2 for the right and 1.107 g/cm^2 for the left humeral shaft.

Figure 6 displays typical X-ray images of the left and right humerus. The bone mass density of the humerus shaft in the left upper arm was determined to be 1.107 g/cm^2. Remarkably, the right humerus displayed a 24% higher bone mass density index of 1.369 g/cm^2.

3. Results

The results of the finite element growth analysis described in section 2.3 are summarized in the sequel.

3.1. *Phase II - Maximum external shoulder rotation*

Figure 7 displays the temporal evolution of the density profile in response to the muscles forces of phase (II) at maximum external shoulder rotation. This phase of the service is crucial in preparation for a high speed serve, see Noffal (1999). It is dominated by an eccentric pre-stretch of the internal rotators that aims at storing elastic energy in the pectoralis major and the latissimus dorsi. In fact, the external shoulder rotation during phase (II) is so extreme that the related posture can only be achieved dynamically. The primary goal is to recover the stored muscle energy during the concentric phase of muscle shortening prior to ball impact and thereby maximize racket acceleration.
According to Elliott et al. (1995), 40 % of the racket velocity can be attributed to upper arm internal rotation. Not surprisingly, this load case generates significant

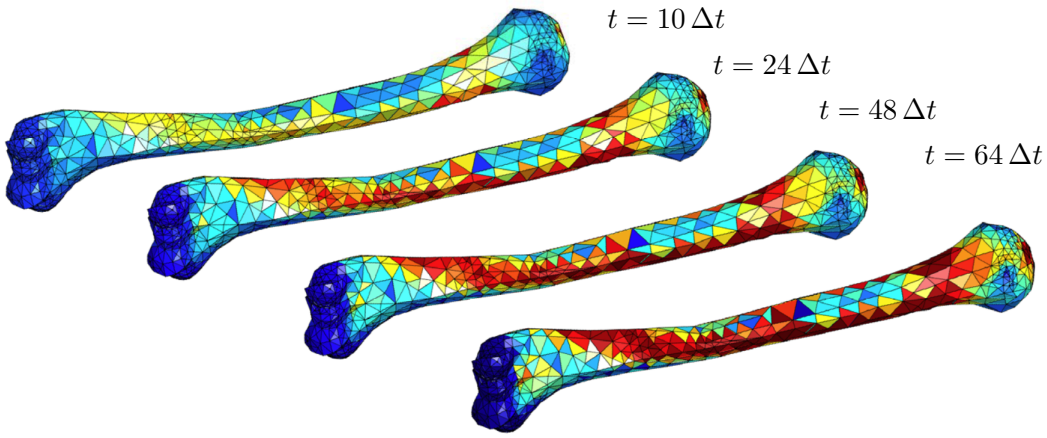

Figure 7. Twisted growth: Time sequence of density adaptation in response to critical muscle loads during phase (II) maximum external shoulder rotation. Red colors indicate significant increase in bone mass density due to overload. Predominant torsional loading by pectoralis major and latissimus dorsi induces humeral hypertrophy with pronounced twisted bone growth.

muscle forces which, in turn, initiate humeral hypertrophy. The tremendous forces of 1490 N and 1275 N generated by the pectoralis major and the latissimus dorsi group severely exceed the physiological baseline level. The computational simulation thus predicts twisted bone growth as a natural consequence of this loading pattern. The density profiles of figure 7 clearly display the characteristic twisted bone growth profile that was found in tennis players, baseball pitchers and handball players. Torsion induced humeral hypertrophy generates increased bone growth all along the humeral axis. The computationally predicted density profiles agree with experimental findings and thus suggest that maximum external shoulder rotation indeed plays a significant role in the functional adaptation process of high performance tennis players.

3.2. *Phase III - Ball impact*

Figure 8 displays the temporal evolution of bone density caused by the muscle forces of phase (III) at ball impact. This phase was previously postulated to generate most critical loads for humeral hypertrophy, see Krahl et al. (1994). It is primarily dominated by the deltoid muscle group with a maximum force of 1600 N that is almost aligned with the humeral axis. In comparison with the previous analysis, the pre-stretch of the pectoralis major and the triceps is released from 1490 N to 1170 N and from 1250 N to 580 N, respectively. Consequently, the overall effect of density growth in response to overload is less pronounced for the isolated consideration of phase (III). A comparison of figures 7 and 8 is in good agreement with this reasoning. Figure 8 displays a density increase along the longitudinal axis of the humerus. However, this increase is less pronounced than the twisted growth of figure 7.

Not only the overall magnitude of bone growth but also the locations of bone deposition differ significantly for both loading scenarios. While bone mass is clearly increased in a torsional pattern all along the humeral shaft in figure 7, new bone is only deposited locally around the attachment points of the deltoid and the pectoralis major in figure 8. Counterintuitively, ball impact thus does not seem to generate the most critical loading for the humeral hypertrophy. During ball impact, muscle forces are aligned with the longitudinal axis of the humerus. From a structural mechanics point of view, the humerus acts as a truss that is primarily loaded in tension. When it comes to structural overload and bone failure, torsional

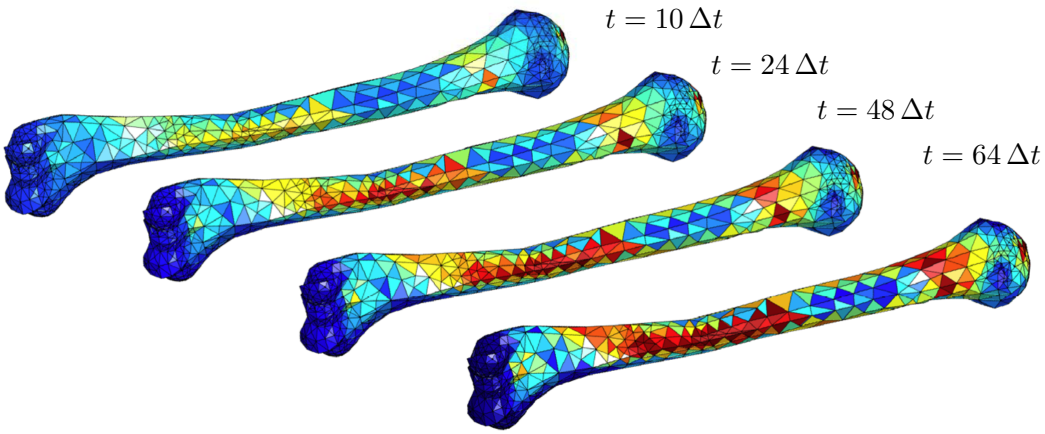

Figure 8. Longitudinal growth: Time sequence of density adaptation in response to critical muscle loads during phase (III) ball impact. Red colors indicate significant increase in bone mass density due to overload. Predominant axial loading by deltoid induces humeral hypertrophy with pronounced bone growth along the longitudinal axis.

loading during phase II seems to be more critical than longitudinal loading during phase III.
In summary, the density profiles predicted with the finite element analysis are in qualitatively good agreement with biophysical reasoning and provide additional insight and improved understanding of complex phenomena associated with torsional growth along the humeral shaft.

4. Discussion

Motivated by athlete college tennis players who reported pain in their dominant shoulder, we initiated a multilevel series of studies including high speed video analysis, musculoskeletal analysis, finite element growth analysis and X-ray bone density analysis. The underlying general hypothesis that overload causes changes in bone density is not new and several computational tools to predict density patterns have developed in the past. The accurate computational bone density prediction, however, crucially relies on reliable techniques to determine the relevant muscle forces that act as phenomenological driving force for the density redistribution process. We propose to determine these forces with the help of the open source software tool OpenSim. We present the case study of one particular tennis player to analyze his personal kinematic chain during the serve, identify his critical postures, determine the relevant muscle groups based on his personal kinematics and predict his personal bone growth profile.
The first step of the analysis is the high speed video analysis which allowed to identify four phases during service: (I) backswing, (II) maximum external shoulder rotation (III) ball impact and (IV) maximum internal shoulder rotation. Critical muscle forces are postulated to occur during phase (II) maximum external shoulder rotation and phase (III) ball impact. Based on the kinematic postures generated during these critical phases, a musculoskeletal analysis was performed to identify four representative muscle groups acting on the humerus during serve: deltoid, latissmus dorsi, pectoralis major and triceps. The musculoskeletal analysis revealed the relevant force vectors, magnitudes and attachment points. For the sake of convenience, each muscle group was then collectively summarized in a single representative muscle force vector.
The critical muscle forces for the critical scenarios of (II) maximum external shoulder rotation and (III) ball impact were applied as external loads in a nonlinear

finite element analysis. To this end, we developed a problem specific finite element tool capable of predicting local changes in density in response to loading. The underlying conceptual framework that allows for such changes is referred to as the thermodynamics of open systems: Regions of local overload are predicted to undergo bone hypertrophy while bone is removed in regions of local underload. Structurally different density patterns were generated by the two critical loading scenarios. Maximum external shoulder rotation was found to induce a global twisted bone growth pattern around the longitudinal humeral axis. In contrast to that, ball impact caused a less pronounced increase of bone density with material being deposited locally near characteristic muscle attachment points. The predicted density profiles were finally compared with bone mass density measurements based on X-ray analysis. The X-ray images revealed a significant increase of bone density in the right upper arm. The bone mass density index of the humeral shaft was found to be 24 % higher in the dominant right arm as compared to non-dominant left arm. These values represent the average bone mass density of the entire humerus shaft. Since bone adaptation is an extremely local phenomenon that primarily affects selected regions of bone, we conclude that the local density increase is significantly higher than just one fourth. Although the remarkable difference in bone mineral density in both arms is clearly caused by intense overload during training, it would be interesting to compare the dominant and non-dominant arms of non-athletes to identify which fraction of the 24% bone mass density increase could truly be attributed to high performance training.

The present manuscript provides insight into the critical loads during high performance training and the related mechanisms that drive skeletal adaptation. As such, the encouraging results of our case study could be of equal benefit to high performance athletes and patients with degenerative bone diseases. They bear the potential to develop patient-specific, optimized new effective training strategies to promote targeted bone growth and thereby improve performance while at the same time reducing risk of chronic injury and overuse pain. Since growth and turnover are most pronounced in early stages of development, the present analyses might be particularly useful in the design of training strategies in early childhood, in particular when identifying optimal timing for individual training strategies in close correlation with skeletal development.

Remarkably, the four phases of the tennis service are almost identical to the four phases of baseball pitching: (I) stride foot contact, (II) maximum external shoulder rotation, (III) ball release and (IV) maximum internal shoulder rotation. It is thus not surprising that professional baseball pitchers exhibit similar bone growth patterns and suffer from the same chronic shoulder pain as tennis players. We thus believe that our analysis tools initially suggested for high performance tennis players could equally well be applied to athletes who perform similar unilateral kinematic motion such as baseball pitchers or handball players.

Overall, there is a more general potential to the present study and its social impact is not exclusively restricted to improve performance in competitive sports. The described techniques to initiate bone growth through strategically targeted overload can provide guidelines to develop patient-specific training schedules for the elderly population. As such, the present theory could help to design physical therapies to increase bone mineral density in treatment of degenerative bone diseases such as osteoporosis.

Although the results of the present study are extremely promising, we would like to point out that there are several limitations to the proposed strategy. In addition to the fact that the chosen finite element mesh is rather coarse and a finer mesh is likely to predict a smoother density profile, we would like to clarify that the

displayed density profile is only based on integration point based density values on the visible elements. To be able to compare the predicted density pattern with real X-ray images, density values would have to be projected onto the X-ray scanning plane. The development of a robust and efficient projection algorithm is part of our current research. The resulting projected density images could eventually be used for a qualitative comparison of local bone mass density indices, which, in turn, would require a local evaluation of the X-ray images.

Since the underlying finite element mesh of our analysis is relatively coarse, the initial bone was assumed to be homogeneous with similar material properties in each element. With a finer mesh, however, we would suggest to model the outer element layer as cortical bone and all internal elements as trabecular bone. Cortical bone would then have a higher initial density than trabecular bone and its density would not be allowed to change over time. An additional advantage of a finer mesh would be that muscle forces could be applied more accurately: The four representative force vectors should eventually be replaced by the individual muscle forces of each muscle group. These changes are straightforward and do not require additional algorithmic modifications or computational cost.

The exact representation of appropriate boundary conditions, however, is a critical issue that cannot be solved straightforwardly. In analogy to most growth and remodeling analyses, we model the tissue as an isolated structure that, apart from a few Dirichlet boundary conditions, is free to move and grow in space. An accurate representation of the in vivo loading situation would require the incorporation of surrounding tissue through an elastic foundation. In such an approach, which is commonly applied in geomechanical modeling, soft environmental support could be accounted for through elastic springs.

Up to now, we base our work purely on a static kinematic analysis. For the sake of simplicity, we ignore arm segment mass, tennis racket mass, forces due to gravity and forces due to the impact impulse of the ball and racket. Since the musculoskeletal analysis tool OpenSim is suited to dynamic analyses, dynamic forces could straightforwardly be incorporated, provided appropriate motion capture data of the service was available. We assume that service dynamics severely influence the critical loads and, accordingly, the predicted density profiles of the humerus.

Apart from these incremental refinements, we believe that the proposed multilevel analysis strategy has a significant potential to provide further understanding of the effects of sport induced muscular overload on skeletal development and functional adaptation.

Acknowledgements

The present research was initiated within the Stanford graduate class ME337 'Mechanics of Growth'. The computational tools are provided as open source software within SimTK at `https://simtk.org` as part of Simbios, the NIH Center for Biomedical Computation at Stanford the support of which we gratefully acknowledge. In addition, we would like to thank Jeff A. Zeller for agreeing to provide his data as a case study.

References

T. J. Chandler, W. B. Kibler, B. Wooten, A. Kiser, and E. Stone. Flexibility comparisions in junior elite tennis players to other athletes. *Am. J. Sports Medicine*, 18:134–136, 1990.

H. Krahl, U. Michaelis, H. G. Pieper, G. Quack, and M. Montag. Simulation of bone-growth through sports – A radiologic investigation of the upper extermities in professional tennis players. *Am. J. Sports Medicine*, 22:751–757, 1994.

H. Haapasalo, S. Kontulainen, H. Sievanen, P. Kannus, M. Jarvinen, and I. Vuori. Exercise-induced bone gain is due to enlargement in bone size without a change in volumetric bone density: A peripheral quantitative computed tomography study of the upper arms of male tennis players. *Bone*, 27:351–357, 2000.

G. Ducher, D. Courteix, S. Meme, C. Magni, J. F. Viala, and C. L. Benhamou. Bone geometry in response to long-term tennis playing and its relationship with muscle volume: A quantitative magnetic resonance imaging study in tennis players. *Bone*, 37:457–466, 2005.

B. C. Elliott. Biomechanics and tennis. *Brit. J. Sports Medicine*, 40:392–396, 2006.

M. B. Sabick, R. Torry, Y.-K. Kim, and R. J. Hawkins. Humeral torque in professional baseball pitchers. *Am. J. Sports Medicine*, 32:892–898, 2004.

D. C. Osbahr, D. L. Cannon, and K. P. Speer. Retroversion of the humerus in the throwing shoulder of college baseball pitchers. *Am. J. Sports Medicine*, 30: 347–353, 2002.

H.-G. Pieper. Humeral torsion in the throwing arm of handball players. *Am. J. Sports Medicine*, 26:247–252, 1998.

B. C. Elliott, G. Fleisig, R. Nicholls, and R. Escamilia. Technique effects on upper limb loading in the tennis serves. *J. Sci. Med. Sport*, 46:76–87, 2003.

B. C. Elliott, R. N. Marshall, and G. Noffal. Contributions of upper limb segment rotations during the power serve in tennis. *J. Appl. Biomech.*, 11:433–442, 1995.

J. Hill. Epidemiologic perspective on shoulder injuries. *Clin. Sport Med.*, 2:241–246, 1983.

P. D. McCann and L. U. Bigliani. Shoulder pain in tennis players. *Sports Medicine*, 17:53–64, 1994.

G. J. Noffal. Where do high speed tennis serves come from? In B. C. Elliott, B. Gibson, and D. Knudson, editors, *Applied Proceedings of the XVII International Symposium on Biomechanics in Sports: Tennis*, pages 27–34. Edith Cowan University Press, Perth, Australia, 1999.

V. E. Krahl. The torsion of the humerus: Its localization, cause and duration in man. *Am. J. Anatomy*, 80:275–319, 1947.

H. H. Jones, J. D. Priest, HAYES W. C., Tichenor C. C., and D. A. Nagel. Humeral hypertrophy in response to exercise. *J. Bone Joint Surgery - American Volume*, 59:204–208, 1977.

S. C. Cowin and D. H. Hegedus. Bone remodelling I: Theory of adaptive elasticity. *J. Elasticity*, 6:313–326, 1976.

S. C. Cowin. Bone remodeling of diaphyseal surface by torsional loads: Theoretical predictions. *J. Biomechanics*, 20:1111–1120, 1987.

G. S. Beaupré, T. E. Orr, and D. R. Carter. An approach for time–dependent bone modelling and remodelling. *J. Orthop. Res.*, 8:651–670, 1990.

T. P. Harrigan and J. J. Hamilton. Optimality condition for finite element simulation of adaptive bone remodeling. *Int. J. Solids & Structures*, 29:2897–2906, 1992.

C. R. Jacobs, M. E. Levenston, G. S. Beaupré, J. C. Simo, and D. R. Carter. Numerical instabilities in bone remodeling simulations: The advantages of a node–based finite element approach. *J. Biomechanics*, 28:449–459, 1995.

D. R. Carter and G. S. Beaupré. *Skeletal Function and Form – Mechanobiology of Skeletal Development, Aging and Regeneration.* Cambridge University Press, 2001.

E. Kuhl and P. Steinmann. Mass– and volume specific views on thermodynamics

for open systems. *Proceedings of the Royal Society of London*, 459:2547–2568, 2003a.

E. Kuhl and P. Steinmann. Theory and numerics of geometrically non–linear open system mechanics. *Int. J. Num. Meth. Eng.*, 58:1593–1615, 2003b.

E. Kuhl and F. Balle. Computational modeling of hip replacement surgery: Total hip replacement vs. hip resurfacing. *Technische Mechanik*, 25:107–114, 2005.

E. Kuhl, A. Menzel, and P. Steinmann. Computational modeling of growth: A critical review, a classification of concepts and two new consistent approaches. *Comp. Mech.*, 32:71–88, 2003.

S. L. Delp, F. C. Anderson, A. S. Arnold, P. Loan, A. Habib, C. T. John, E. Guendelman, and D. G. Thelen. OpenSim: Open-source software to create and analyze dynamic simulations of movement. *IEEE Transactions on Biomedical Engineering*, 54:1940–1950, 2007a.

S. L. Delp, C. T. John, E. Guendelman, F. C. Anderson, and A. Habib. OpenSim: Open-source software within SimTK. *Simbios NIH Center for Biomedical Computation at Stanford*, `https://simtk.org/home/opensim`, 2007b.

E. Kuhl. SimGrowth: 0pen-source software within SimTK. *Simbios NIH Center for Biomedical Computation at Stanford*, `https://simtk.org/home/simgrowth`, 2007.

K. R. S. Holzbaur, W. M. Murray, and S. L. Delp. A model of the upper extremity for simulating musculoskeletal surgery and analyzing neuromuscular control. *Annals Biomed. Eng.*, 33:829–840, 2005.

K. R. S. Holzbaur, W. M. Murray, G. E. Gold, and S. L. Delp. Upper limb muscle volumes in adult subjects. *J. Biomechanics*, 40:742–749, 2007.

T. P. Harrigan and J. J. Hamilton. Finite element simulation of adaptive bone remodelling: A stability criterion and a time stepping method. *Int. J. Num. Meth. Eng.*, 36:837–854, 1993.

D. R. Carter and W. C. Hayes. The behavior of bone as a two–phase porous structure. *J. Bone Jt. Surgery*, 59-A:785–794, 1977.

L. J. Gibson and M. F. Ashby. *Cellular Solids*. Cambridge University Press, 2nd edition, 1997.